How to cite: *Angew. Chem. Int. Ed.* **2023**, e202306061
doi.org/10.1002/anie.202306061

Fluorescent Probes

Spontaneously Blinking Rhodamine Dyes for Single-Molecule Localization Microscopy

Weijie Chi, Davin Tan, Qinglong Qiao, Zhaochao Xu, and Xiaogang Liu**

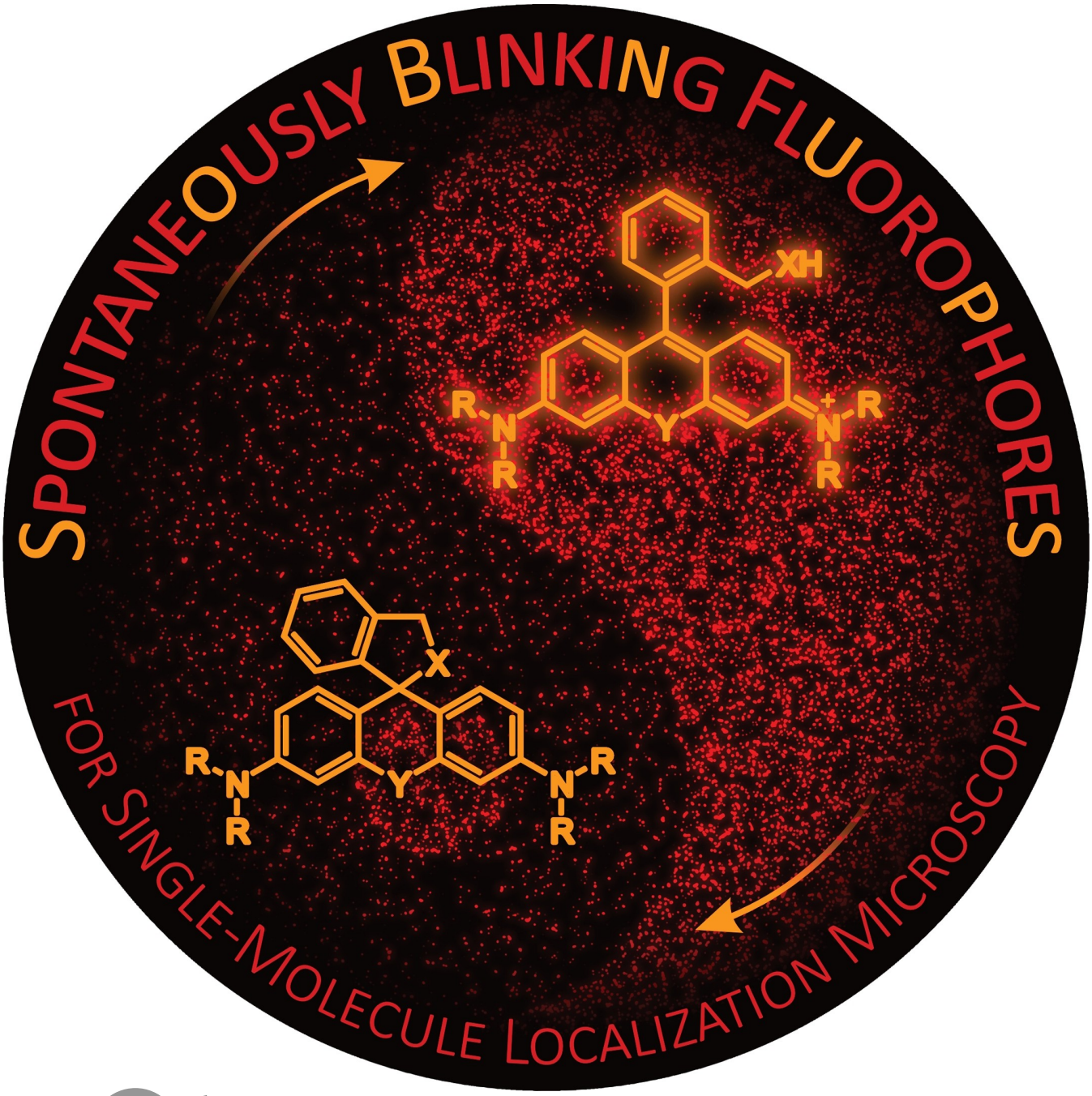

Abstract: Single-molecule localization microscopy (SMLM) has found extensive applications in various fields of biology and chemistry. As a vital component of SMLM, fluorophores play an essential role in obtaining super-resolution fluorescence images. Recent research on spontaneously blinking fluorophores has greatly simplified the experimental setups and extended the imaging duration of SMLM. To support this crucial development, this review provides a comprehensive overview of the development of spontaneously blinking rhodamines from 2014 to 2023, as well as the key mechanistic aspects of intramolecular spirocyclization reactions. We hope that by offering insightful design guidelines, this review will contribute to accelerating the advancement of super-resolution imaging technologies.

1. Introduction

In 2014, the Nobel Prize in Chemistry was jointly awarded to Eric Betzig, Stefan Hell, and William E. Moerner for their groundbreaking work in "super-resolution fluorescence microscopy." Super-resolution fluorescence microscopy (or nanoscopy) surpasses the diffraction limit of approximately 200 nm, providing a powerful imaging technique for directly visualizing the dynamic changes in living cells with unprecedented resolution (at around 20 nm).[1] One major approach to achieve super-resolution imaging is through single-molecule localization. Based on this approach, numerous imaging techniques have been developed, such as photoactivated localization microscopy (PALM), stochastic optical reconstruction microscopy (STORM), and point accumulation for imaging in nanoscale topography (PAINT). These single-molecule localization microscopies (SMLM) have been extensively applied in various frontier fields of biology and medical research, including the study of cell-mediated immune responses and tomographical analysis of cancer cells. This, in turn, has greatly accelerated many research areas, such as drug discovery.[2]

In SMLM, individual fluorophores are temporally separated by continually switching between "dark" and "bright" states, allowing a sparse set of emitters to be captured and localized in each camera frame.[3–5] Three main methods have been developed to achieve "sparse emissions" and "stochastic switching," where most of the fluorophores are converted to dark states, and only a small subset of these dyes randomly switch to the fluorescent state. In the first method, an intense visible laser or additives are used to bleach most of the fluorophores into dark states, followed by stochastic transitions to the bright states for imaging (Figure 1a). In the second method, when (nearly) all fluorophores are in a dark state, additional UV or blue photoactivation light is required to enable random and sparse emissions before these bright fluorophores switch back to the dark state (Figure 1b).[6] The third method, currently achievable only with certain rhodamine derivatives, involves a "spontaneous" thermal equilibrium between a small population of the open form (the fluorescent state) and a large population of the closed form (the dark state) (Figure 1c). The fluorescent and dark states rapidly interconvert through a reversible intramolecular spirocyclization reaction, resulting in a spontaneously blinking phenomenon (Figure 1d).

The first two methods are often not ideal, as they require intense high-power and/or short-wavelength laser irradiation or additives, potentially causing phototoxicity issues and affecting cellular physiology. Moreover, commonly used organic dyes for SMLM, such as Cy5 and Alexa647, have low membrane permeability and are not suitable for live-cell imaging.[7] In contrast, the third method avoids these issues as it does not necessitate high-power laser irradiation or chemical additives, significantly simplifying experimental setups. The spirocyclization reactions in spontaneously blinking rhodamines also help to improve cellular permeability.[8] Besides, spontaneously blinking rhodamines offer the advantage of enabling long-lasting super-resolution imaging. In this context, developing spontaneously blinking rhodamines and analogs holds considerable potential for super-resolution imaging.

In this review, we summarize recent advances in the development of spontaneously blinking rhodamine dyes (from 2014 to 2023). Our discussion focuses on the current state-of-the-art molecular design strategies and potential future directions for developing spontaneously blinking rhodamines with enhanced photophysical properties. Ultimately, we hope this review will effectively facilitate the creation of multi-colored spontaneously blinking dyes and significantly aid in advancing super-resolution dynamic imaging in live cells.

2. Spontaneously blinking rhodamines

2.1. Discovery and applications of HMSiR derivatives

The first spontaneously blinking rhodamine dye was reported by the Urano group in 2014.[9] In their work, pK_{cycl} was adopted as an important parameter to screen potential candidates. pK_{cycl} refers to the pH value at which the absorbance of rhodamine (in the first UV/Vis-NIR absorption band) decreases to half of its maximum. A large pK_{cycl}

[*] Prof. W. Chi
Collaborative Innovation Center of One Health, School of Science, Hainan University
Renmin Road 58, Haikou 570228 (P. R. China)
Prof. W. Chi, Dr. D. Tan, Prof. X. Liu
Fluorescence Research Group, Singapore University of Technology and Design
8 Somapah Road, 487372, Singapore (Singapore)
E-mail: xiaogang_liu@sutd.edu.sg
Prof. Q. Qiao, Prof. Z. Xu
CAS Key Laboratory of Separation Science for Analytical Chemistry, Dalian Institute of Chemical Physics, Chinese Academy of Sciences
457 Zhongshan Road, Dalian 116023 (China)
E-mail: zcxu@dicp.ac.cn

value denotes a high population of rhodamine molecules in the fluorescent open form under physiological conditions (i.e., pH 7.4). For example, when the $pK_{cycl} > 8.5$, most fluorophores exist in the open form at pH 7.4. In contrast, when the $pK_{cycl} < 6$, a small number of fluorophores would be in the open form, and most would exist in the non-fluorescent closed form at pH 7.4.

After screening various compounds, **HMSiR** (Figure 2a) was identified as the best candidate for SMLM, due to its suitable pK_{cycl} (5.8) and relatively long lifetime in the open form (0.245 s). Additionally, the peak UV/Vis-NIR absorption and fluorescence wavelengths of **HMSiR** ($\lambda_{abs}/\lambda_{em} = 650/671$ nm in aqueous solution) are in the near-infrared region. The molar absorption coefficient (ε) and fluorescence quantum yield (ϕ) of **HMSiR** is 100 000 $M^{-1}cm^{-1}$ and 0.39 in water, respectively, demonstrating good brightness ($\varepsilon \times \phi = 39\,000\ M^{-1}cm^{-1}$). However, the photon count per switching event of HMSiR was ≈2600, which is slightly lower than those for conventional fluorophores (such as Alexa647 with 3500 photons).[10] Finally, Urano and co-workers demonstrated that the spontaneously blinking rhodamine is favored for SMLM cellular imaging and can be used to track the motion of organelles in living cells at a low illumination power of only 40 $W cm^{-2}$. They demonstrated that the motion of microtubules could be monitored with an excellent spatial resolution during the 30–60 min observation window with **HMSiR** (Figure 2b).

Following this work, three additional milestone works extended the utility of **HMSiR** for cellular super-resolution imaging. In 2017, Toomre and co-workers further shifted the fluorescence ON/OFF ratio of **HMSiR** to ultra-low values by placing **HMSiR** in a hydrophobic environment, such as within organelle membranes.[11] They designed and synthesized an environment-sensitive membrane probe (**HMSiR-Tz**, Figure 2c). When selectively tagged to the membrane using biorthogonal tetrazine chemistry, the authors were able to conduct a three-dimensional study of endoplasmic reticulum dynamics in a live cell using SMLM (Figure 2d). Their results demonstrated that super-resolution imaging with a long time-lapse could be achieved by increasing the labeling density and reducing the ON/OFF ratio of **HMSiR** in a hydrophobic environment.

Weijie Chi received his PhD degree under the supervision of Prof. Zesheng Li from the Beijing Institute of Technology, China in 2017. He worked as a research fellow in Prof. Xiaogang Liu's group at Singapore University of Technology and Design, Singapore since 2017. In 2021, he started his independent career in the School of Science at Hainan University where he is now a full professor. His research interests include computational chemistry, fluorescent dye, organic semiconductor, and high energy density low sensitivity materials.

Davin Tan received his BSc degree at the National University of Singapore (2010). He obtained his MSc degree in Chemical Science at King Abdullah University of Science and Technology (2012) in Saudi Arabia with Prof. Kuo-Wei Huang, and his PhD degree in Chemistry at McGill University (2017) in Canada with Prof. Tomislav Friščić. He is now expanding his research interest and is working with Prof. Xiaogang Liu at the Singapore University of Technology and Design to develop fluorescent dyes.

Qinglong Qiao received his BSc in 2012 and PhD in 2017 from Dalian University of Technology. He then joined Prof. Zhaochao Xu's lab at the Dalian Institute of Chemical Physics in 2018 and became an Associate Professor in 2020. His research interests include the development of new fluorophores, dynamic super-resolution imaging, and fluorescent probes for proteins.

Zhaochao Xu received his PhD degree from the Dalian University of Technology under the supervision of Prof. Xuhong Qian in 2006. Subsequently, he joined Prof. Juyoung Yoon's group at Ewha Womans University as a postdoctoral researcher. Since October 2008, he was a Herchel Smith Research Fellow at the University of Cambridge in Prof. David R. Spring's group. In 2011, he moved to the Dalian Institute of Chemical Physics as a Professor. His research is focusing on the development of fluorescent probes for super-resolution fluorescence imaging.

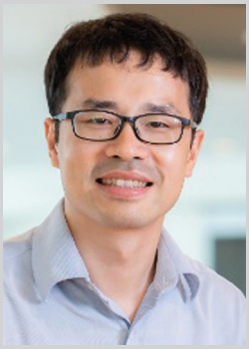

Xiaogang Liu is an Assistant Professor at the Singapore University of Technology and Design (SUTD). He obtained his Ph.D. degree from the University of Cambridge under the supervision of Professor Jacqueline Cole in 2014. He was a SMART Scholar with Singapore-MIT Alliance for Research and Technology (2014–2017). After joining SUTD in 2017, he led the Fluorescence Research Group to research the structure–property relationships of organic dyes, as well as develop high-performance fluorescent products for a wide range of applications.

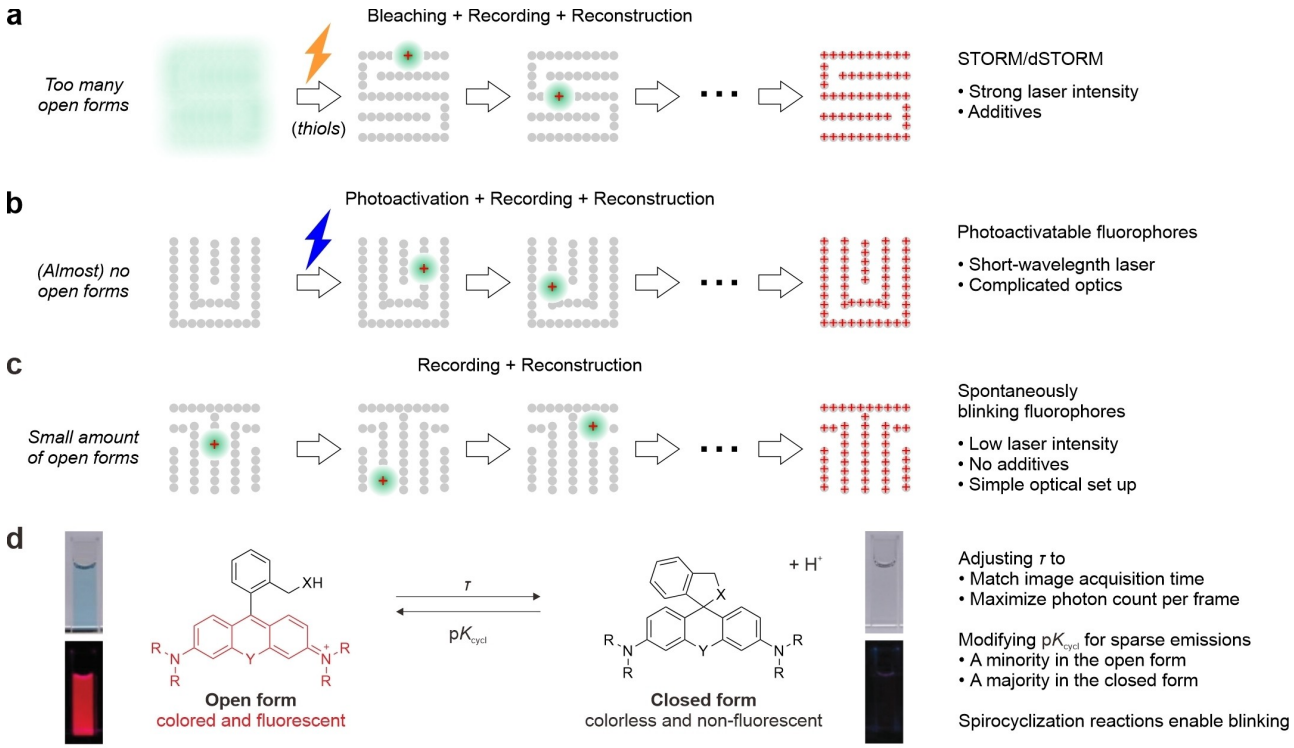

Figure 1. a)–c) Three popular methods for achieving single-molecule localization imaging using various rhodamine dyes with different degrees of ring-opening tendencies. d) Thermal equilibrium of spirocyclization reactions between the open form (fluorescent) and the closed form (non-fluorescent). pK_{cycl} is the equilibrium constant for the spirocyclization reaction and τ is the lifetime of the open form. The inset in d) shows the photographs of the dye solution under ambient light (top) and UV light (bottom) in the open form and the closed form, respectively. d) is adapted from Reference [9].

Subsequently, in 2020, Wombacher's group reported a new spontaneously blinking **HMSiR** derivative, ***f*-HMSiR** ($\lambda_{abs}/\lambda_{em}=654/670$ nm; Figure 2e), created by directly coupling the tetrazine group to **HMSiR**.[12] The molar extinction coefficient and fluorescence quantum yield of ***f*-HMSiR** is 45000 $M^{-1}cm^{-1}$ and 0.06 at pH 3.5, respectively, resulting in low brightness ($\varepsilon\times\phi=2700\ M^{-1}cm^{-1}$). The low fluorescence quantum yield is due to the attachment of the tetrazine quencher.[13,14] ***f*-HMSiR** exhibited a low pK_{cycl} of 4.0. However, after bioorthogonal reactions at the tetrazine moiety, the product molecule displayed the desired pK_{cycl} (5.2). The λ_{abs} (653 nm) and λ_{em} wavelengths (669 nm) of the product molecule are almost the same as those of ***f*-HMSiR**.

Importantly, the molar extinction coefficient and fluorescence quantum yield of the product increased to 185000 $M^{-1}cm^{-1}$ and 0.26, respectively, resulting in high brightness ($\varepsilon\times\phi=48100\ M^{-1}cm^{-1}$). Moreover, prolonged SMLM imaging experiments were conducted, enabling a detailed study of mitochondria dynamics at sub-diffraction resolution (Figure 2f).

The third significant study is from Lukinavičius and coworkers, who designed a spontaneously blinking cell-permeable rhodamine dye (**HMSiR-tubulin**; $\lambda_{abs}/\lambda_{em}=659/673$ nm; Figure 2g) by optimizing the ligand and linker.[15] However, **HMSiR-tubulin** showed a lower pK_{cycl} than **HMSiR** due to the attachment of the large linker group and the corresponding modification of the local environment. **HMSiR-tubulin** also exhibited good biocompatibility and effective cell staining, enabling the observation of microtubule dynamics (growing and shrinking) over 4 minutes in SMLM (Figure 2h). Notably, by utilizing MINFLUX nanoscopy (which employed a patterned laser excitation beam), Lukinavičius et al. achieved an impressive ≈2.3 nm localization precision of microtubules with **HMSiR-tubulin**.

Additionally, the Rivera-Fuentes group applied the single-molecule blinking pattern of **HMSiR** in conjunction with a deep-learning algorithm to identify peptides.[16] The advantage of this method is the ability to distinguish peptide segments with different sequences.

In summary, SMLM imaging based on spontaneously blinking rhodamines has attracted increasing attention from various fields in recent years.

2.2. The development of spontaneously blinking hydroxyalkyl rhodamines

Four years after the introduction of **HMSiR**, the Urano group developed the first green-light-emitting spontaneously blinking rhodamine (**HEtetTFER**; $\lambda_{abs}/\lambda_{em}=507/530$ nm) in 2018 (Figure 3a).[17] They designed **HEtetTFER** by substituting the hydroxymethyl group with a more electron-donating and bulkier hydroxyethyl group. **HEtetTFER** has a high ε and ϕ (80000 $M^{-1}cm^{-1}$ and 0.76, respectively), resulting in

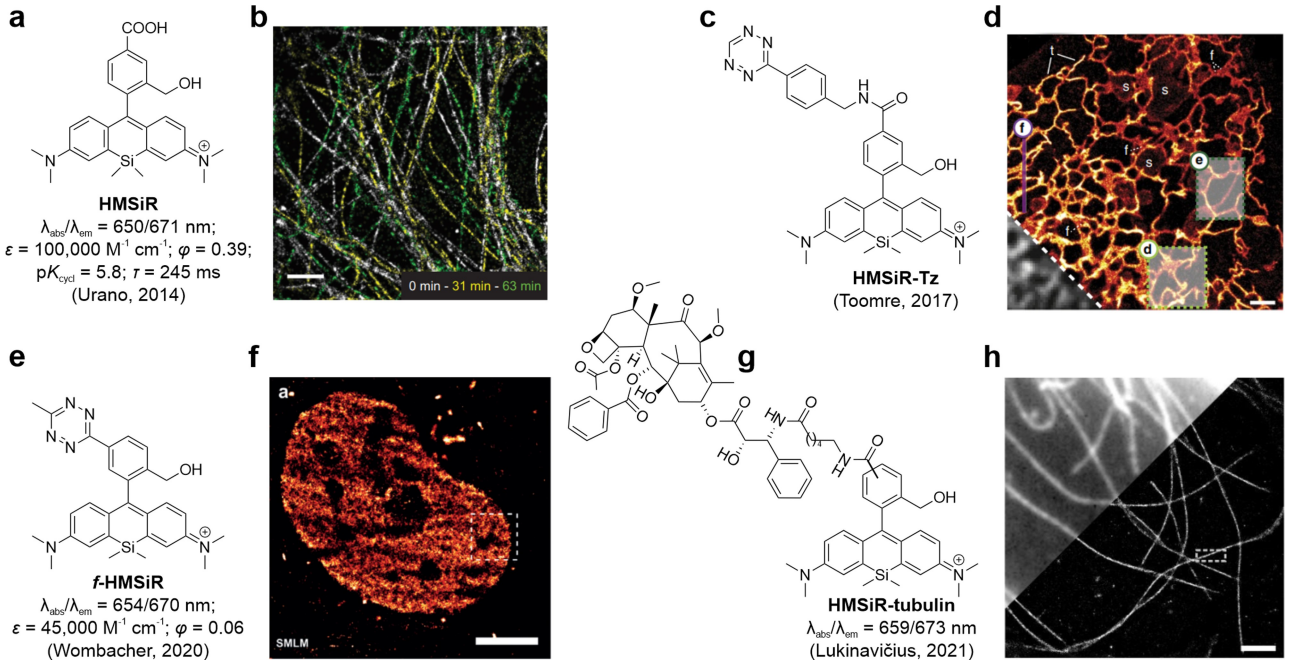

Figure 2. a) Molecular structures and photophysical properties of **HMSiR**. b) Sequential acquisition of super-resolution images of microtubules at 0 min (white), 31 min (yellow), and 63 min (green). Excitation at 647 nm with a laser power density of 40 W cm^{-2}. Each super-resolution image was reconstructed from 1000 images (30 ms/frame) corresponding to an acquisition time of 30 s. Scale bar: 2 μM. c) Molecular structure of **HMSiR-Tz**. d) Super-resolution imaging of the endoplasmic reticulum in a live HeLa cell over 25 min; the image was reconstructed from 800 frames recorded over 2 s and Kalman-filtered. ⟨s⟩: sheet-like ER, ⟨f⟩: fenestrated endoplasmic reticulum sheets, ⟨t⟩: tubular endoplasmic reticulum. Laser intensity: 9.9 kW cm^{-2}. Scale bar: 1 μm. e) Molecular structures and photophysical properties of ***f*-HMSiR**. f) ***f*-HMSiR** reveals cellular dynamics in live HeLa cells with improved resolution; HeLa cells transiently expressing H2 A-HaloTag were incubated with HTL-BCN (10 μM), washed, and labeled with ***f*-HMSiR** (2 μM). g) Molecular structures and photophysical properties of **HMSiR-tubulin**. h) Imaging of microtubules in living and fixed U-2 OS cells stained with **HMSiR-tubulin**; living cells were stained with 100 nM **HMSiR-tubulin** and imaged without washing at 100 Hz with a 640 nm laser at 0.4 kW cm^{-2} excitation power. The image was reconstructed from 2500 frames. b), d), f), and h) are adapted from References [9, 11, 12] and [15], respectively.

enhanced brightness ($\varepsilon\times\phi = 60800\ M^{-1}cm^{-1}$) compared to **HMSiR** ($\varepsilon\times\phi = 39000\ M^{-1}cm^{-1}$). With a p$K_{cycl}$ value of 5.5, **HEtetTFER** exhibits spontaneously blinking ability. The photon count per switching event is 1145.6 ± 968. Simultaneously using both **HMSiR** and **HEtetTFER** enabled a dual-color SMLM image of microtubules and mitochondria in fixed Vero cells in an additive-free buffer solution (Figure 3b).

In 2019, the Lavis group established a quantitative K_{L-Z} framework for developing fluorogenic and spontaneously blinking rhodamines, leading to the identification of a yellow spontaneously blinking fluorophore (**HM-JF$_{526}$**; $\lambda_{abs}/\lambda_{em}$ = 526/550 nm; Figure 3c).[18] **HM-JF$_{526}$** labeling yielded 571 photons on average with a 25 nm localization accuracy during SMLM imaging of microtubules (Figure 3d). It also demonstrated good compatibility with standard immunolabeling protocols.

In 2020, the Urano group rationally designed the first spontaneously blinking carbon-rhodamine dye (**HMCR550**; $\lambda_{abs}/\lambda_{em}$ = 559/582 nm; Figure 3e) using molecular modeling.[19] **HMCR550** has a quantum yield of 0.65 and displays an ideal pK_{cycl} value (5.4) with a sufficient open form lifetime (40.9 ms). Urano and colleagues demonstrated live-cell SMLM using **HMCR550** with a HaloTag ligand (Figure 3f).

In 2020, Liu, Xu, and co-workers quantitatively designed and synthesized two spontaneously blinking rhodamines: **HM-DS655** ($\lambda_{abs}/\lambda_{em}$ = 655/669 nm) and **HM-DS531** ($\lambda_{abs}/\lambda_{em}$ = 531/555 nm; Figure 3g).[20] The fluorescence brightness of **HM-DS655** ($\varepsilon\times\phi = 41280\ M^{-1}cm^{-1}$) was measured to be 21 % brighter than that of **HMSiR** ($\varepsilon\times\phi = 34100\ M^{-1}cm^{-1}$, as per their in-house measurements). **HM-DS531** also displayed outstanding brightness ($\varepsilon\times\phi = 65250\ M^{-1}cm^{-1}$). Both **HM-DS655** and **HM-DS531** had a pK_{cycl} value of 5.3. Single-molecule fluorescent analysis showed open form lifetimes of approximately 90 ms for **HM-DS655** and 50 ms for **HM-DS531** in PMMA films. The average photon number of a single **HM-DS655** molecule per frame was 1387. Liu et al. demonstrated the use of **HM-DS655** for both in vitro and in vivo super-resolution imaging applications (Figure 3h, i).

Schepartz and co-workers reported a near-infrared (NIR) spontaneously blinking rhodamine dye, **Yale$_{676sb}$** ($\lambda_{abs}/\lambda_{em}$ = 676/694 nm; Figure 3j).[21] **Yale$_{676sb}$** exhibited a considerable quantum yield (0.59) and had a pK_{cycl} value of 5.9 with an open form lifetime of 4.5 ms. The authors demonstrated that live-cell SMLM imaging of the endoplasmic reticulum could be performed with **Yale$_{676sb}$** (Figure 3k). Due to the red-shifted spectra, **Yale$_{676sb}$** can work with

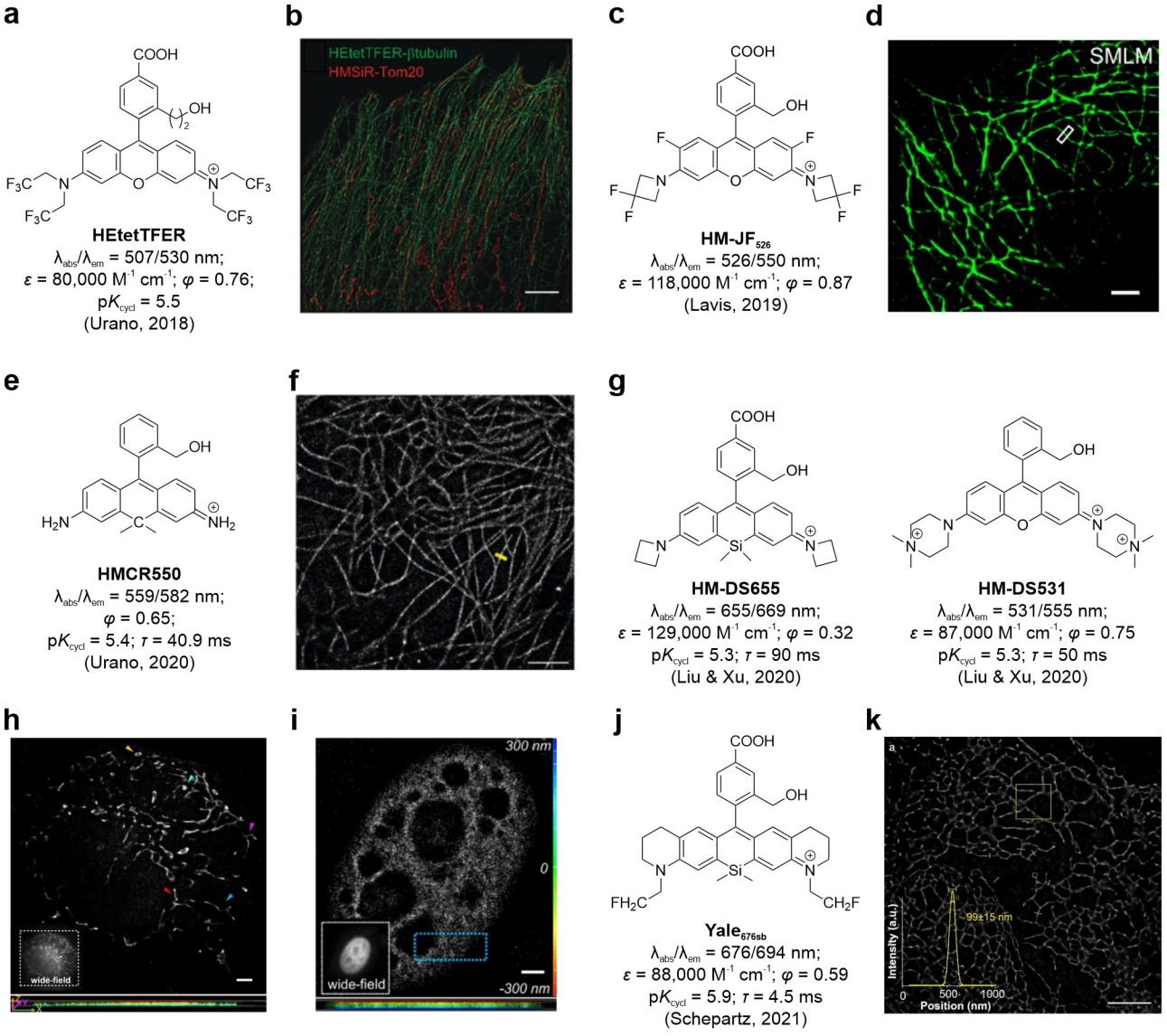

Figure 3. a) Molecular structure and photophysical properties of **HEtetTFER**. b) Dual-color SMLM of microtubules (**HEtetTFER**) and mitochondria (**HMSiR**) in fixed Vero cells. Scale bar: 5 μm. c) Molecular structure and photophysical properties of **HM-JF$_{526}$**. d) SMLM image of microtubules with functionalized **HM-JF$_{526}$**. Scale bar: 5 μm. e) Molecular structures and photophysical properties of **HMCR550**. f) Live-cell SMLM of β-tubulin-HaloTag in Vero cells with functionalized **HMCR550**. Super-resolution image was reconstructed from 1000 frames (15 ms per frame). Excitation at 561 nm (400 W cm^{-2}). Scale bar: 3 μm. g) Molecular structures and photophysical properties of **HM-DS655** and **HM-DS531**. h) 3D-STORM imaging of mitochondria with functionalized **HM-DS655** in fixed HeLa cells expressing SNAP-Cox8A. Inset: Wide-field imaging of mitochondria in fixed HeLa cells. i) 3D-STORM imaging of a nucleus with functionalized **HM-DS655** in a live HeLa cell expressing SNAP-H2B. Inset: Wide-field imaging of the nucleus. Scale bar: 2 μm. j) Molecular structures and photophysical properties of **Yale$_{676sb}$**. k) Super-resolution image of the ER in U2-OS cells using **Yale$_{676sb}$**. The average reconstructed signal as a function of position along the seven-line profiles indicated by yellow lines is shown. Scale bars: 5 μm. b), d), f), h), i), k) is adapted from References [17–21].

HMSiR to achieve dual-color SMLM imaging of intracellular organelles in live cells.

2.3. The progress of spontaneously blinking spirolactam rhodamines

In addition to hydroxymethyl rhodamines, spirolactam rhodamines have shown great potential as spontaneously blinking dyes. In 2018, Tetin et al. reported the first spontaneously blinking spirolactam rhodamine, **FRD-B** ($\lambda_{abs}/\lambda_{em}$ = 560/583 nm; Figure 4a).[22] **FRD-B** had a lower pK_a (≈4.3) and exhibited sparse emission at pH 7.4. The average open form lifetime was 0.6 s. **FRD-B** was suitable for observing static or slow-moving structures using SMLM, such as immunostained fixed cells (Figure 4b).

In 2021, Xiao et al. reported a clickable spontaneously blinking spirolactam rhodamine, **Atto565-Tet** (Figure 4c).[23] **Atto565-Tet** had a slightly higher pK_a (5.2) than **FRD-B**. After bioorthogonal reactions with bicyclo[6.1.0]non-4-yne,

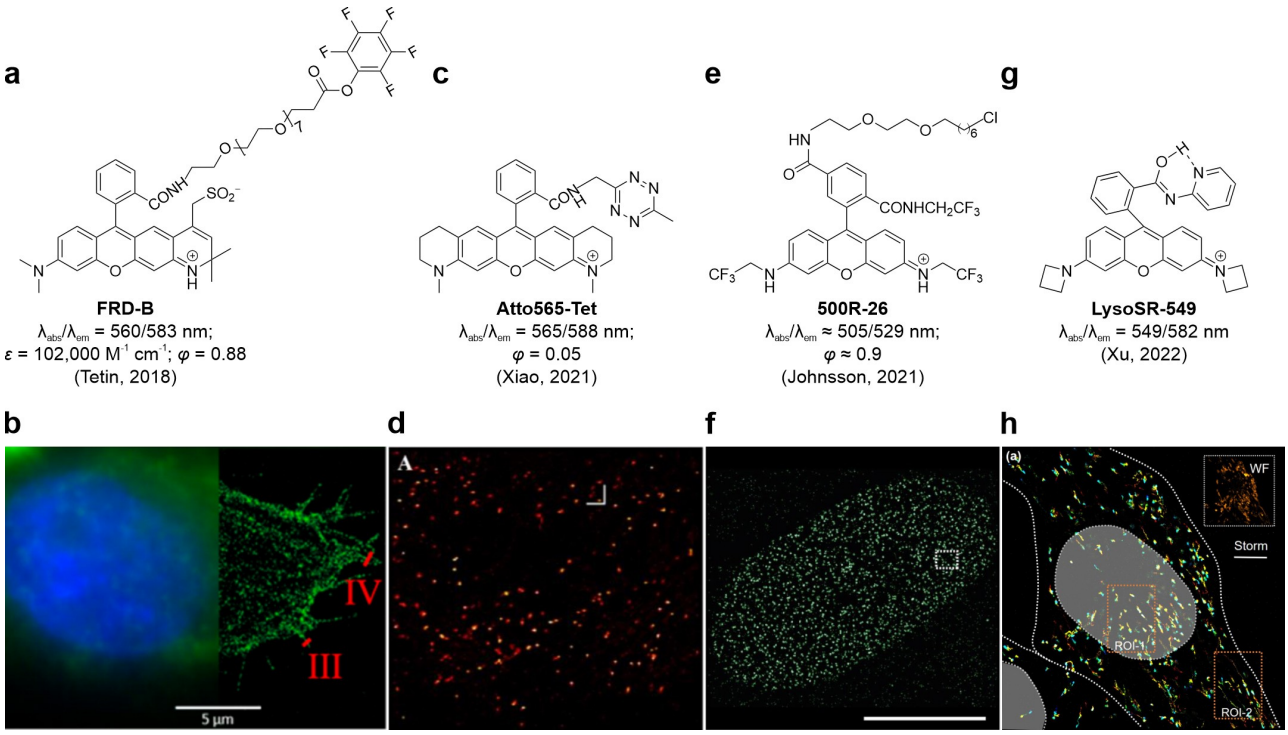

Figure 4. a) Molecular structures and photophysical properties of **FRD-B**. b) STORM super-resolution imaging using **FRD-B**. Scale bar: 5 μm. c) Molecular structures and photophysical properties of **Atto565-Tet**. d) **Atto565-Tet** used for super-resolution imaging of lysosomes in live HeLa cells. Scale bar: 3 μm. e) Molecular structure of **500R-26**. f) Super-resolution image of endogenously tagged Nup96-Halo in fixed U-2 OS cells labeled with **500R-26**. Scale bar: 10 μm. g) Molecular structures and photophysical properties of **LysoSR-549**. h) Long-term SMLM imaging of whole-cell lysosomes with **LysoSR-549** in live HeLa cells. Scale bar: 5 μm. Inset: Wide-field imaging. b), d), f), and h) is adapted from References [22–25].

the reaction product of **Atto565-Tet** exhibited a high quantum yield of 0.46 at pH 4.2. Xiao et al. demonstrated SMLM imaging of key mitochondrial structures using **Atto565-Tet** without any UV irradiations or external thiol additives. **Atto565-Tet** was also successfully deployed for SMLM imaging of acidic organelles (e.g., lysosomes) with a resolution of ≈22 nm (Figure 4d).

Johnsson et al. reported a spontaneously blinking spirolactam rhodamine, **500R-26** (Figure 4e), by converting the ortho-carboxy group of the rhodamine into alkylamides.[24] They investigated the blinking characteristics of **500R-26** and its performance in SMLM imaging via endogenously Nup96-Halo tagging in fixed U-2 OS cells (Figure 4f). **500R-26** showed excellent spontaneously blinking properties, with an average photon count of 631 per localization and a peak localization precision of 8.9 nm.

In 2022, Xu et al. introduced an ortho-methylpyridine moiety into the spirolactam scaffold and designed **LysoSR-549** ($\lambda_{abs}/\lambda_{em}$ = 549/582 nm; Figure 4g).[25] With a low pK_{cycl} value of 3.2, **LysoSR-549** displayed spontaneous blinking in acidic lysosomes, enabling super-resolution imaging with high spatial and temporal resolution. The probe allowed for simultaneous and dynamic quantification of pH values in all lysosomes in the entire cell at the single lysosome level (Figure 4h). Using **LysoSR-549**, Xu et al. resolved whole-cell lysosome subpopulations based on lysosome distributions, sizes, and luminal pH.

In 2023, Hell et al. designed six spontaneously blinking rhodamine dyes, **H1**–**H6** (Figure 5a).[26] These dyes were prepared from silicon rhodamines with modified meso-aromatic rings, displaying spontaneously blinking behavior with NIR emissions (680–690 nm) and moderate fluorescence quantum yields (0.10–0.24). The results showed that benzothiophene-derived dyes **H1**–**H3** generally have shorter open form (bright-state) lifetimes and longer dark state lifetimes than thiophene derivatives **H4**–**H6**. Hell et al. collected MINFLUX images of Megfp-Nup107 (Figure 5b) and U2OS-Nup96-Halo (Figure 5c) fixed cells labeled with a derivative of **H4**. They showed that spontaneously fast-blinking fluorophores can accelerate the development of MINFLUX nanoscopy.

2.4. The development of spontaneously blinking sulfonamide rhodamines

In 2023, Xiao et al. designed and synthesized four spontaneously blinking sulfonamide rhodamine dyes, namely **STMR**, **SRhB**, **PySRh**, and **PiSRh** (Figure 6a–d).[27,28] The UV/Vis absorption peaks of these rhodamine dyes range from 537 to 561 nm, with emission peaks between 580 and 596 nm. These dyes displayed moderate fluorescence quantum yields (0.12–0.15). Interestingly, although **STMR**, **SRhB**, and **PySRh** exhibited larger pK_{cycl} values (6.91–7.34)

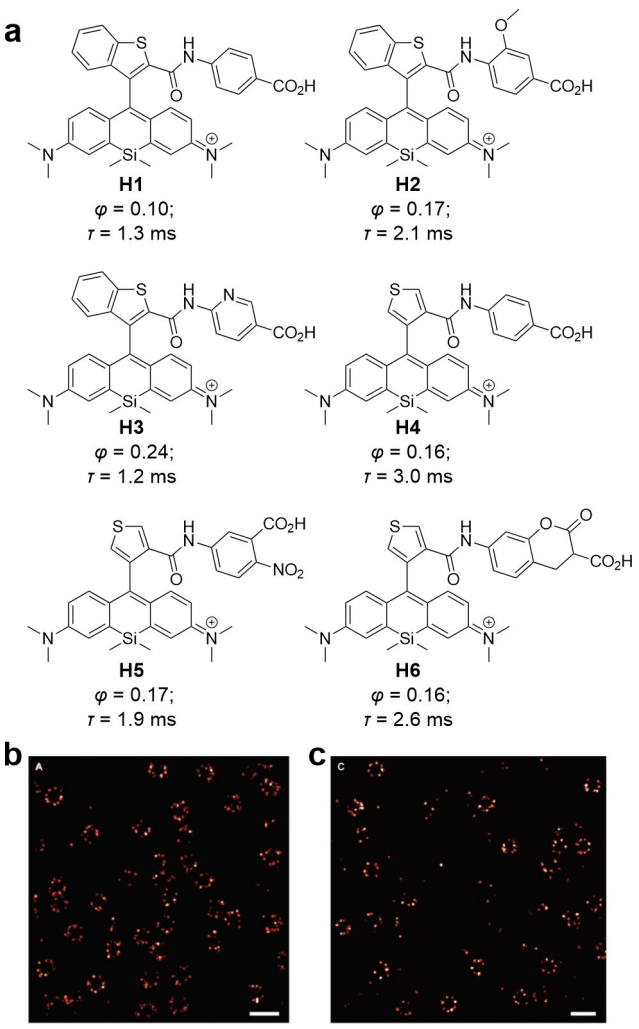

Figure 5. a) Molecular structures and photophysical properties of **H1**–**H6**. b) MINFLUX images of fixed Megfp-Nup107 cells labeled with the derivative of **H4**. c) MINFLUX images of fixed U2OS-Nup96-Halo cells labeled with the derivative of **H4**. Scale bar: 200 nm. b), c) is adapted from Reference [26].

compared to **PiSRh** ($pK_{cycl} = 5.05$), they possess spontaneously blinking properties with suitable lifetimes (25–112 ms). They achieved super-resolution imaging of living cells labeled with **STMR** (Figure 6e), **SRhB** (Figure 6f), **PySRh** (Figure 6g), and **PiSRh** (Figure 6h) through HaloTags. Importantly, they proposed a new parameter (recruiting rate) to reveal the natural switching frequency of spirocyclic equilibrium.

To this end, Liu et al. highlighted that the pK_{cycl} window for spontaneous blinking is not rigid. The exact requirements of pK_{cycl} depend on various factors, such as local polarity, labeling density, and the environment's acidity. Additionally, changing the ring-locking group will shift the spontaneously blinking window due to distinct pH titration curves with different slopes.[20]

Both pK_{cycl} and recruiting rate are important parameters for assessing spontaneously blinking dyes. pK_{cycl} (a thermodynamic parameter) reflects the proportion of fluorescent species in the open form, while the recruiting rate captures the switching dynamics between fluorescent and dark species. Considering both parameters provides valuable insights for selecting dyes with desired blinking behavior.

3. Factors controlling the intramolecular spirocyclization equilibrium

Managing the intramolecular spirocyclization equilibrium and kinetics of rhodamines is crucial for achieving optimal spontaneous blinking (Figure 7a). For successful super-resolution imaging, only a small proportion of rhodamines should remain in the fluorescent open form to ensure sparse emissions; these rhodamines must also display suitable open form lifetimes to synchronize with image acquisition and gather enough photons during the switching cycles.[29] These spirocyclization properties, combined with high quantum yields, excellent photostability, and biocompatibility, make rhodamine derivatives highly favored for super-resolution imaging applications.

Recently, Liu et al. proposed a unified push-pull model to explain the intramolecular spirocyclization reactions of rhodamines.[30] They systematically examined both intrinsic and external factors' effects on altering the spirocyclization reactions of 17 rhodamine dyes (Figure 7b). They demonstrated that intrinsic factors, such as increasing the electron-donating strength (or decreasing the vertical ionization potential) of R_1 or changing R_2 from silicon to carbon/oxygen, can significantly lower the energy barriers and shift the spirocyclization equilibrium towards the open form (Figure 7c, d), resulting in a higher population of open form species. Enhancing the electron-withdrawing strength of R_3 and R_4 also strengthens the push-pull effect, stabilizing and populating the open forms of rhodamines (Figure 7e).

Besides these intrinsic factors, external factors also significantly influence the spirocyclization equilibrium. A high-polarity solvent can boost the push-pull effect and stabilize the charge-separated open form rhodamines through potent dipole-dipole interactions. For instance, the relative Gibbs free energy of the open form of compound **1** (compared to the closed form) in DMSO is lower than in diethyl ether and tetrahydrofuran (Figure 7f).

Furthermore, the solvent's hydrogen-donating ability (α) has a more substantial impact on promoting the ring-opening reaction than solvent polarity (π^*). Liu et al. discovered a strong linear relationship (Figure 7g) between the difference in Gibbs free energy of the closed and open forms of compound **1** and the solvent polarity scale (π^*) and the solvent hydrogen-donating ability (α). The absolute coefficient of α (0.48) is 12 times larger than that of π^* (0.04), highlighting the importance of hydrogen-donating ability in facilitating ring-opening reactions.

To investigate the impact of hydrogen bonds on spirocyclization reactions, explicit water molecules were positioned near a rhodamine dye during computational modeling. The findings revealed that hydrogen bond interactions significantly lowered the transition state energy

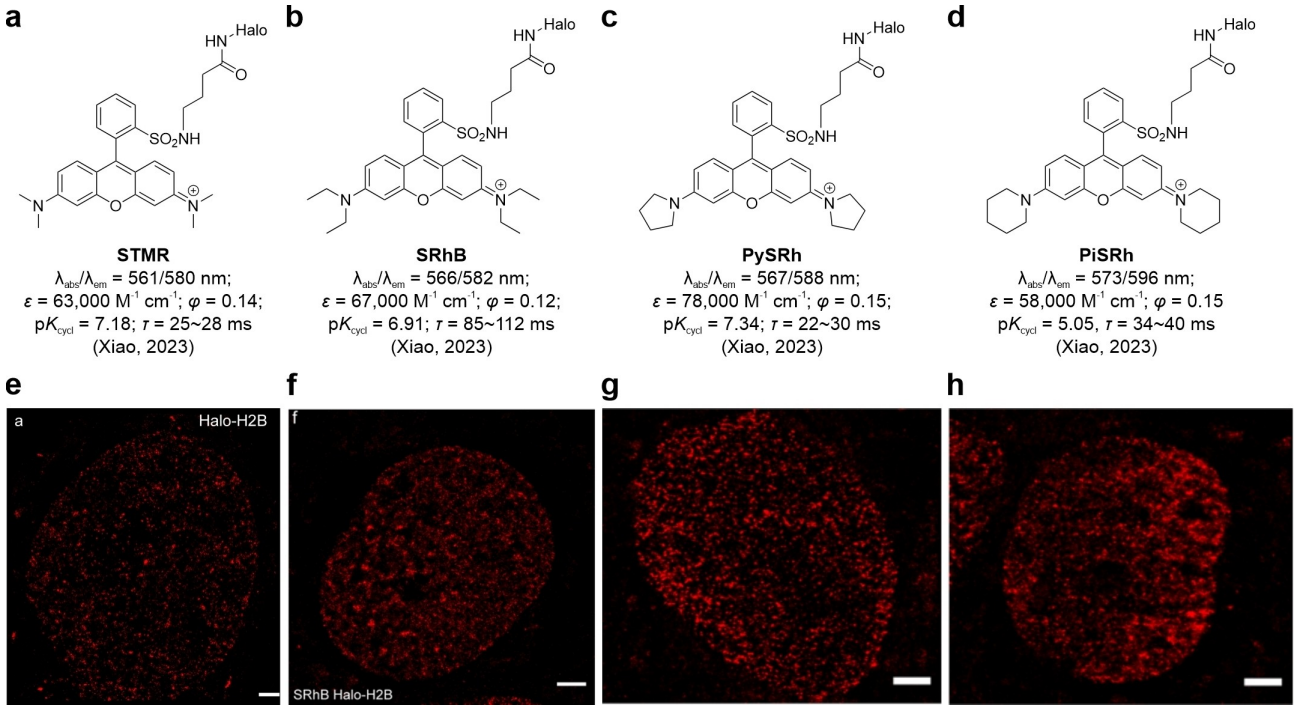

Figure 6. a)–d) Molecular structures and photophysical properties of **STMR**, **SRhB**, **PySRh**, and **PiSRh**. e)–f) Super-resolution imaging of living cells labeled with **STMR**, **SRhB**, **PySRh**, and **PiSRh** through HaloTags, respectively. Scale bars: 1 μm (e, g) and 2 μm (f, h). e), f), g), and h) is adapted from References [27, 28].

barriers of the forward ring-opening reaction and stabilized the open form of rhodamines (Figure 7h).

Moreover, Lin and colleagues demonstrated that an R_4 group with substantial steric hindrance could facilitate the conversion from the closed form to the open form.[31] This conclusion is also supported by Harbron's study.[32] These outcomes are not unexpected, as the ring-opening reaction minimizes steric repulsion, and increasing steric hindrance promotes ring-opening reactions.

These computational and experimental investigations highlight the significance of both intrinsic molecular designs and external environmental factors in adjusting the spirocyclization equilibrium of rhodamines. This understanding offers valuable insights into the rational design of rhodamines with tailored spirocyclization properties.

4. Experimental and theoretical methods for predicting the blinking properties of rhodamines

4.1. Methods for characterizing the spirocyclization equilibrium

Two experimental methods have been proposed to quantify the spirocyclization equilibrium. The first method, proposed by the Urano group, is based on pK_{cycl}.[9] According to their findings, a pK_{cycl} of less than 6 represents a suitable threshold value to ensure sparse emissions of rhodamines in most cellular environments (Figure 8a).

Another method for describing the spirocyclization equilibrium is the lactone-zwitterion equilibrium constant ($K_{L\text{-}Z}$), used by Lavis and many other groups [Eq. (1)].[8,18] A low $K_{L\text{-}Z}$ value indicates that most rhodamines are in the closed form.

$$K_{L\text{-}Z} = (\varepsilon_{dw}/\varepsilon_{max})/(1-\varepsilon_{dw}/\varepsilon_{max}) \quad (1)$$

where ε_{dw} is the absorption coefficient of the rhodamine, i.e., in a 1:1 (v/v) dioxane: water binary mixture containing 0.01 % (v/v) of triethylamine. The ε_{max} value represents the maximum absorption coefficient (i.e., when all rhodamines are in the open form).

pK_{cycl} tends to be more reliable than $K_{L\text{-}Z}$ in screening spontaneously blinking rhodamines. This is because sparse open form rhodamines have a very low absorbance, which often cannot be measured accurately using a standard UV/Vis spectrometer.

In addition to experimental methods, two theoretical methods have been proposed to predict the spirocyclization equilibrium. Urano demonstrated that the intramolecular equilibrium of hydroxymethyl (HM rhodamine) and aminomethyl (AM rhodamine) rhodamine derivatives involves an acid-base equilibrium (Figure 8b).[33] They assumed that only four species participate in the equilibrium, including the open forms under acidic and basic conditions (O_A and O_B) and closed forms under acidic and basic conditions (C_A and C_B).

The pK_{cycl} can be interpreted as the pH at which the concentration of open forms ($O_A + O_B$) is equal to that of

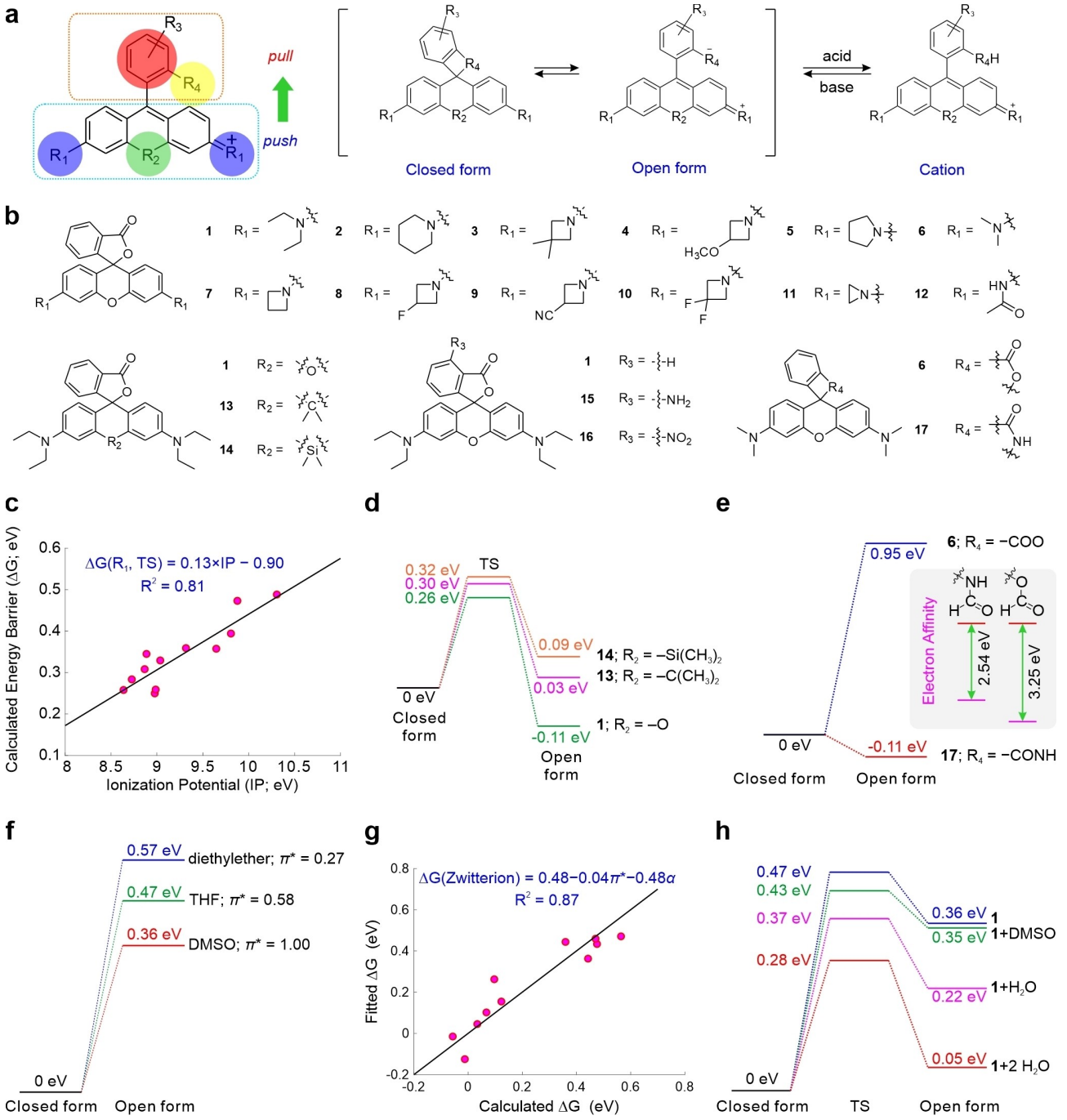

Figure 7. a) Illustration of representative substitution sites on rhodamine derivatives that affect lactone-zwitterion-cation equilibrium. b) Molecular structures of **1**–**17**. c) The change in energy barriers ΔG (R_1, TS) during the ring-opening reactions as the ionization potential of the R_1 group increases. d) Relative Gibbs free energy of the closed form, transition states (TS), and open form of **1**, **13**, and **14** in water, as a function of R_2. e) Relative Gibbs free energy of the closed and open forms of **6** and **17** in water, as a function of R_4. The inset displays the electron affinity (EA) of $HCOO^{\bullet}$ and $HCONH^{\bullet}$ radicals in vacuo to quantify the electron-withdrawing strength of R_4. f) Relative Gibbs free energy of the closed and open forms of **1** in three solvents with different polarities (π^*). g) Correlations between calculated and fitted relative Gibbs free energy values between the closed and open forms of **1** [ΔG(**1**, zwitterion)] in 11 solvents. h) Relative Gibbs free energy of the closed form, transition states (TS), and open form of **1** and its complexes **1** + DMSO, **1** + H_2O, and **1** + 2 H_2O in DMSO. This figure is adapted from Reference [30].

closed forms ($C_A + C_B$). The pK_{cycl} values can then be represented by Equations (2)–(4):

$$pK_{cycl} = log\frac{K_A - 1}{K_{aNH} - K_{aOH}K_A} \quad (2)$$

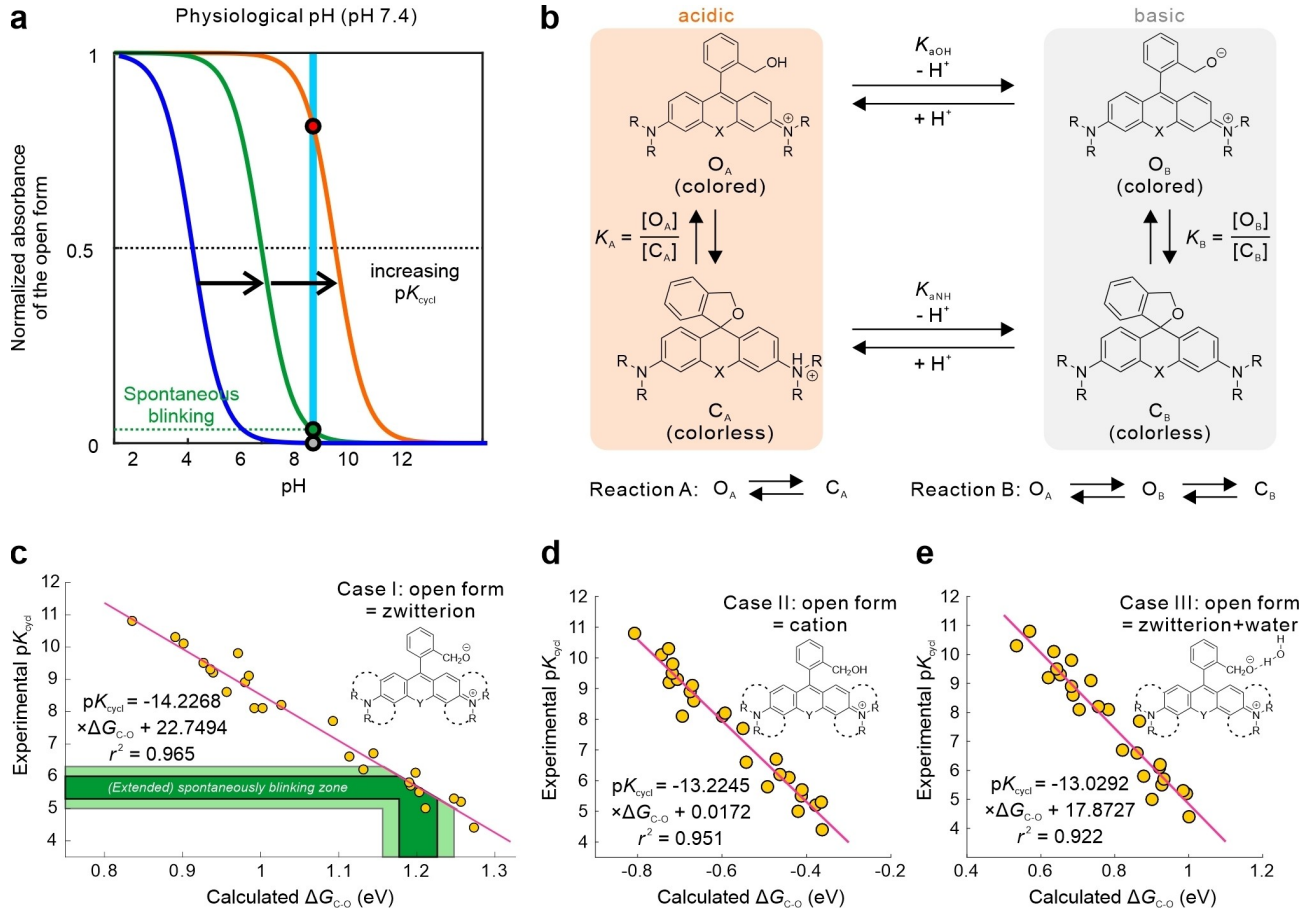

Figure 8. a) Schematic pH titration curves of rhodamine derivatives with pK_{cycl} of 6.0 (blue), 7.4 (green), and 8.5 (orange). b) Model mechanism of the ring-closing reaction of hydroxymethyl derivatives. c)–e) Correlations between calculated $\Delta G_{C\text{-}O}$ and experimental pK_{cycl} values for a series of hydroxymethyl rhodamine dyes reported by the Urano group. Three types of open forms were considered during calculations: c) zwitterion, d) cation, and e) zwitterion + water. a), c)–e) is adapted from Reference [20], and b) is adapted from Reference [33].

$$K_A = \exp(-\frac{\Delta G}{RT}) \quad (3)$$

$$\Delta G = G(O_A) - G(C_A) \quad (4)$$

In Equation (2), the K_{aNH} and K_{aOH} values are determined from experimental data. K_A is calculated using Equation (3), in which ΔG is the difference in Gibbs free energy between the open form and the closed form of rhodamine under acidic conditions (O_A and C_A, respectively).

As hydrogen bonding between rhodamines and water plays a critical role in the spirocyclization reactions, Urano et al. included explicit water molecules in their quantum chemical calculations to obtain reliable ΔG values. Their calculations showed that when three explicit water molecules are added to the model, calculated pK_{cycl} values can match experimental results. This method shows great potential for predicting the pK_{cycl} values of unknown rhodamines. However, this methodology is not a "pure" theoretical predictor because two parameters, namely K_{aNH} and K_{aOH}, are extracted from experimental data.

Another approach is based on a quantitative structure–property relationship (QSPR), as reported by Liu and Xu et al.[20] They collected experimental pK_{cycl} values for 28 existing hydroxymethyl rhodamine dyes and calculated the ΔG values of these rhodamines. Here, ΔG refers to the difference in Gibbs free energy between the open and closed forms of rhodamines. They considered three different open forms: (1) zwitterion, (2) cation (upon protonation), and (3) zwitterion and water complex (to consider hydrogen bonding effects). When modeling zwitterions, they discovered an excellent linear correlation ($r^2 = 0.965$) between the calculated ΔG and experimental pK_{cycl} values (Figure 8c). Considering other open forms also leads to excellent correlations with pK_{cycl} values (Figure 8d, e). Furthermore, Liu and Xu suggested that a pK_{cycl} range of [5.3, 6.0] (experimental) is a good indication of spontaneously blinking properties with sparse (but not too few) emissions and a reasonable open form lifetime in (nearly) neutral cellular environments. Considering the prediction error (≈ 0.3), they relaxed the permissible pK_{cycl} range to [5.0, 6.3] (calculated) in their in-silico design of spontaneously blinking rhodamines. Guided by these ΔG threshold values and the discovered pK_{cycl}-ΔG correlation, Liu and Xu et al. designed five spontaneously

blinking hydroxymethyl rhodamines. Two of them have been synthesized and characterized, and the experimental results validated the accuracy of their prediction method.

Liu and Xu's modeling is simpler than Urano's method, but it comes with several approximations. First, the open forms of rhodamines could be in different protonation states (i.e., zwitterions and cations) as a function of pK_{cycl}. However, in Liu and Xu's modeling, the open forms are consistently treated as zwitterions (or cations). This consistent theoretical treatment ensures that the calculated ΔG values of various rhodamines are directly comparable to each other. The resulting excellent ΔG–pK_{cycl} correlations reflect a simple causal relationship: a large ΔG shifts the spirocyclization equilibrium towards the closed form, thus affording a low pK_{cycl} value. However, it does not reflect the true status of the open forms, which could be either zwitterions, cations, or a mixture of both. Second, using only zwitterions in the model does not sufficiently account for hydrogen bonding effects. Liu et al. suggest that these approximations could cause a systematic drift in calculated ΔG values, but it does not affect the accuracy of their prediction method (as reflected by the large r^2 values of ΔG–pK_{cycl} correlations). Nevertheless, they also pointed out that this relationship is only applicable to hydroxymethyl rhodamines, as other ring-locking groups may encounter different environmental interactions and afford differential offsets between the calculated and experimental ΔG.

Despite these shortcomings, the computational methods presented by the Urano group and Liu group could greatly facilitate the further development of spontaneously blinking rhodamine dyes.

4.2. Methods to predict fluorescence lifetime

The open form lifetime (τ) is another critical parameter in the design of spontaneously blinking dyes. A τ value of several to hundreds of milliseconds would match the image acquisition speed and allow for sufficient detection of photons. Urano et al. proposed a theoretical method to determine τ values by calculating the transition state energy barrier ($\Delta G^{\ddagger}$) with consideration of explicit water molecules.[19]

They considered two reaction processes to calculate $\Delta G^{\ddagger}$: a pH-independent process (A) and a pH-dependent process (B; Figure 8b). Their calculations revealed that the most stable transition state structure was obtained when a water molecule bridges the hydroxymethyl group and the amino group in Reaction A. The free energy barrier of Reaction B can be determined as the ring-closing reaction from O_B to C_B. Based on this model, τ can be expressed using the following Equations (5)–(7):

$$\Delta G^{\ddagger}_{A(B)} = G(TS_{A(B)}) - G(O_{A(B)}) \quad (5)$$

$$K_{A(B)} = \exp(-\frac{\Delta G^{\ddagger}_{A(B)}}{RT}) \quad (6)$$

$$\tau \approx \frac{1}{K_A + K_B 10^{pH-pH_{aOH}}} \quad (7)$$

where $\Delta G^{\ddagger}_{A(B)}$) denotes the activation free energy of Reactions A and B from open to closed forms, $K_{A(B)}$ represents the rate of ring-closing reaction. Using these equations, Urano et al. calculated and predicted τ values of existing rhodamines. The calculated results are in good agreement with experimental data, highlighting the robust predictive power of their methodology.

Incorporating explicit solvent molecules and determining the necessary number of solvent molecules in theoretical calculations is challenging. Careful consideration, validation, and cross-checking between predictions and experimental measurements are crucial for extending the success of this method to other dye families.

5. Summary and Outlook

Fluorescent dyes are critical components of SMLM. Spontaneously blinking rhodamines simplify both the optical setup and imaging process, enabling long-lasting super-resolution imaging of live cells without the need for intense laser irradiation or chemical additives. Since Urano's pioneering work in 2014, several spontaneously blinking rhodamine dyes have been reported, but overall research progress remains in its early stages. Addressing several challenges could expedite the development of this important research area.

Firstly, spontaneously blinking rhodamines in the NIR region of >700 nm are still lacking. Long-wavelength dyes could reduce phototoxicity, minimize autofluorescence interference, increase penetration depths, and provide additional possibilities for multicolor imaging. Recently, substantial research efforts have focused on this area by engineering the "bridging" heteroatoms in the xanthene scaffold (using a sulfone group by the Guo group[34] and a phosphine oxide group by the Yamaguchi group[35]) or expanding the π-conjugation (as done by the Yang group[36]). These resulting rhodamines exhibited significant bathochromic shifts, with λ_{em} exceeding 700 or even 800 nm. However, most existing NIR rhodamine derivatives lack a spiro-ring locking group to activate switching between dark and bright states. Further molecular engineering could transform them into spontaneously blinking NIR dyes. This strategy of incorporating a ring-locking group could also be applied to other fluorophore families, such as cyanine dyes. Notably, the Rivera-Fuentes group has successfully developed spontaneously blinking polymethine dyes (Figure 9).[37]

Secondly, researchers should explore new mechanisms beyond spirocyclization to enable spontaneous blinking. The Urano group demonstrated that spontaneous blinking can be achieved through a reversible nucleophilic reaction between intracellular glutathione and a xanthene-based fluorophore in the ground state (Figure 9).[38] Similarly, Yang and colleagues revealed that glutathione could also reduce a Si-rhodamine, resulting in spontaneous blinking

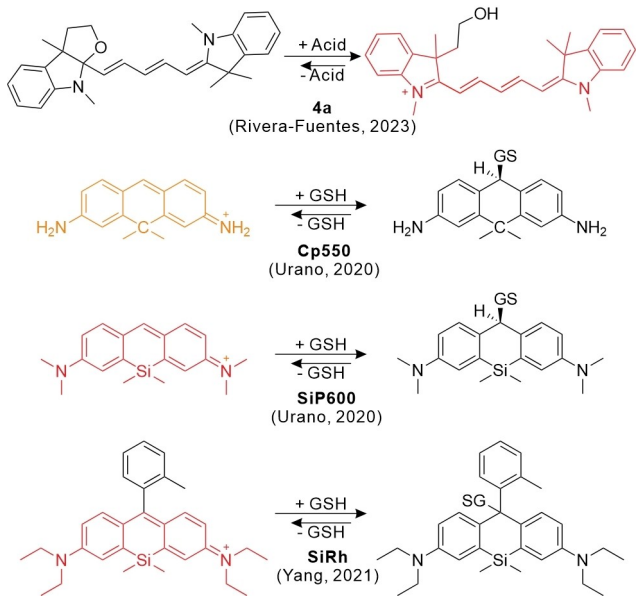

Figure 9. Molecular structures and schematic illustration of the novel blinking mechanisms of fluorophores based on reversible chemical reactions.

(Figure 9).[39] It is also worth noting that the Tang group discovered spontaneous blinking in *o*-TPE-ON+, but the blinking mechanism remains unclear.[40] Investigating these mechanisms (i.e., reversible chemical reactions, aggregation-disaggregation equilibrium, binding-unbinding to biomolecules) could open new avenues for developing a diverse array of spontaneously blinking fluorophores.

Thirdly, theoretical prediction methods for blinking properties (such as spirocyclization equilibrium and open form lifetime) should be further refined. Theoretical calculations play a crucial role in developing spontaneously blinking rhodamine dyes by avoiding trial and error and minimizing experimental costs. Despite the success of reported theoretical methods, these predictions are only applicable to a specific class of rhodamine dyes (hydroxymethyl rhodamines). Substantial effort is needed to develop a more efficient and generalizable method that can encompass a wide range of compounds. In this regard, machine learning has shown significant potential for predicting the thermodynamics and kinetics of organic reactions.[41,42] Combining machine learning with quantum chemical calculations and molecular dynamics simulations, based on extensive experimental data, could greatly assist in calculating switching equilibrium and kinetics for various spontaneously blinking dyes.

In conclusion, this review highlights the recent progress in spontaneously blinking rhodamine research, focusing on the thermodynamics, kinetics of spirocyclization mechanisms, and the photophysical properties of these dyes. We discussed various molecular design strategies and computational methods for screening potential blinking dyes. The advancement of spontaneously blinking dyes necessitates cross-disciplinary research efforts encompassing chemistry, biology, and physics. Through such transdisciplinary collaborations, the development and implementation of spontaneously blinking fluorophores will undoubtedly accelerate the progress and application of super-resolution imaging technologies in numerous exciting fields.

Acknowledgements

We thank A*STAR under its Advanced Manufacturing and Engineering Program (A2083c0051), the Ministry of Education, Singapore (MOEMOET2EP10120-0007), SUTD-ZJU IDEA grant [SUTD-ZJU (VP) 201905], the National Natural Science Foundation of China (22278394, 22078314, 21908216) and Dalian Institute of Chemical Physics (DICPI202227, DICPI202142), Hainan Provincial Natural Science Foundation of China (123MS001), Collaborative Innovation Center Foundation of the Hainan University (XTCX2022JKB03), Research Start-up Fund Project of Hainan University (RZ2200001217), and Tianjin University-Hainan University Independent Innovation Fund (RZ2200003795).

Conflict of Interest

The authors declare no conflict of interest.

Data Availability Statement

Data sharing is not applicable to this article as no new data were created or analyzed in this study.

Keywords: Rhodamine Dyes · Single-Molecule Localization Microscopy · Spirocyclization Equilibrium · Spontaneously Blinking Fluorophores

[1] L. Möckl, D. C. Lamb, C. Bräuchle, *Angew. Chem. Int. Ed.* **2014**, *53*, 13972–13977.
[2] A. Bullen, *Nat. Rev. Drug Discovery* **2008**, *7*, 54–67.
[3] D. Sage, T.-A. Pham, H. Babcock, T. Lukes, T. Pengo, J. Chao, R. Velmurugan, A. Herbert, A. Agrawal, S. Colabrese, A. Wheeler, A. Archetti, B. Rieger, R. Ober, G. M. Hagen, J.-B. Sibarita, J. Ries, R. Henriques, M. Unser, S. Holden, *Nat. Methods* **2019**, *16*, 387–395.
[4] D. Sage, H. Kirshner, T. Pengo, N. Stuurman, J. Min, S. Manley, M. Unser, *Nat. Methods* **2015**, *12*, 717–724.
[5] S. W. Hell, *Science* **2007**, *316*, 1153–1158.
[6] Q. Qi, W. Chi, Y. Li, Q. Qiao, J. Chen, L. Miao, Y. Zhang, J. Li, W. Ji, T. Xu, X. Liu, J. Yoon, Z. Xu, *Chem. Sci.* **2019**, *10*, 4914–4922.
[7] G. T. Dempsey, J. C. Vaughan, K. H. Chen, M. Bates, X. Zhuang, *Nat. Methods* **2011**, *8*, 1027–1036.
[8] J. B. Grimm, A. K. Muthusamy, Y. Liang, T. A. Brown, W. C. Lemon, R. Patel, R. Lu, J. J. Macklin, P. J. Keller, N. Ji, L. D. Lavis, *Nat. Methods* **2017**, *14*, 987–994.
[9] S.-N. Uno, M. Kamiya, T. Yoshihara, K. Sugawara, K. Okabe, M. C. Tarhan, H. Fujita, T. Funatsu, Y. Okada, S. Tobita, Y. Urano, *Nat. Chem.* **2014**, *6*, 681–689.

[10] S. A. Jones, S.-H. Shim, J. He, X. Zhuang, *Nat. Methods* **2011**, *8*, 499–505.
[11] H. Takakura, Y. Zhang, R. S. Erdmann, A. D. Thompson, Y. Lin, B. McNellis, F. Rivera-Molina, S.-N. Uno, M. Kamiya, Y. Urano, J. E. Rothman, J. Bewersdorf, A. Schepartz, D. Toomre, *Nat. Biotechnol.* **2017**, *35*, 773–780.
[12] P. Werther, K. Yserentant, F. Braun, N. Kaltwasser, C. Popp, M. Baalmann, D.-P. Herten, R. Wombacher, *Angew. Chem. Int. Ed.* **2020**, *59*, 804–810.
[13] W. Chi, L. Huang, C. Wang, D. Tan, Z. Xu, X. Liu, *Mater. Chem. Front.* **2021**, *5*, 7012–7021.
[14] T. Shen, W. Zhang, P. Yadav, X. W. Sun, X. Liu, *Mater. Chem. Front.* **2023**, *7*, 1082–1092.
[15] R. T. Gerasimaitė, J. Bucevičius, K. A. Kiszka, S. Schnorrenberg, G. Kostiuk, T. Koenen, G. Lukinavičius, *ACS Chem. Biol.* **2021**, *16*, 2130–2136.
[16] S. Püntener, P. Rivera-Fuentes, *J. Am. Chem. Soc.* **2023**, *145*, 1441–1447.
[17] S.-N. Uno, M. Kamiya, A. Morozumi, Y. Urano, *Chem. Commun.* **2018**, *54*, 102–105.
[18] Q. Zheng, A. X. Ayala, I. Chung, A. V. Weigel, A. Ranjan, N. Falco, J. B. Grimm, A. N. Tkachuk, C. Wu, J. Lippincott-Schwartz, R. H. Singer, L. D. Lavis, *ACS Cent. Sci.* **2019**, *5*, 1602–1613.
[19] R. Tachibana, M. Kamiya, A. Morozumi, Y. Miyazaki, H. Fujioka, A. Nanjo, R. Kojima, T. Komatsu, T. Ueno, K. Hanaoka, T. Yoshihara, S. Tobita, Y. Urano, *Chem. Commun.* **2020**, *56*, 13173–13176.
[20] W. Chi, Q. Qiao, C. Wang, J. Zheng, W. Zhou, N. Xu, X. Wu, X. Jiang, D. Tan, Z. Xu, X. Liu, *Angew. Chem. Int. Ed.* **2020**, *59*, 20215–20223.
[21] J. Tyson, K. Hu, S. Zheng, P. Kidd, N. Dadina, L. Chu, D. Toomre, J. Bewersdorf, A. Schepartz, *ACS Cent. Sci.* **2021**, *7*, 1419–1426.
[22] P. J. Macdonald, S. Gayda, R. A. Haack, Q. Ruan, R. J. Himmelsbach, S. Y. Tetin, *Anal. Chem.* **2018**, *90*, 9165–9173.
[23] Z. Liu, Y. Zheng, T. Xie, Z. Chen, Z. Huang, Z. Ye, Y. Xiao, *Chin. Chem. Lett.* **2021**, *32*, 3862–3864.
[24] N. Lardon, L. Wang, A. Tschanz, P. Hoess, M. Tran, E. D'Este, J. Ries, K. Johnsson, *J. Am. Chem. Soc.* **2021**, *143*, 14592–14600.
[25] Q. Qiao, W. Liu, J. Chen, X. Wu, F. Deng, X. Fang, N. Xu, W. Zhou, S. Wu, W. Yin, X. Liu, Z. Xu, *Angew. Chem. Int. Ed.* **2022**, *61*, e202202961.
[26] M. Remmel, L. Scheiderer, A. N. Butkevich, M. L. Bossi, S. W. Hell, *Small* **2023**, *19*, 2206026.
[27] Y. Zheng, Z. Ye, X. Zhang, Y. Xiao, *J. Am. Chem. Soc.* **2023**, *145*, 5125–5133.
[28] Y. Zheng, Z. Ye, Y. Xiao, *Anal. Chem.* **2023**, *95*, 4172–4179.
[29] S. van de Linde, A. Löschberger, T. Klein, M. Heidbreder, S. Wolter, M. Heilemann, M. Sauer, *Nat. Protoc.* **2011**, *6*, 991–1009.
[30] W. Chi, Q. Qi, R. Lee, Z. Xu, X. Liu, *J. Phys. Chem. C* **2020**, *124*, 3793–3801.
[31] L. Yuan, W. Lin, Y. Feng, *Org. Biomol. Chem.* **2011**, *9*, 1723–1726.
[32] S. G. Stratton, G. H. Taumoefolau, G. E. Purnell, M. Rasooly, W. L. Czaplyski, E. J. Harbron, *Chem. Eur. J.* **2017**, *23*, 14064–14072.
[33] R. Tachibana, M. Kamiya, S. Suzuki, K. Morokuma, A. Nanjo, Y. Urano, *Commun. Chem.* **2020**, *3*, 82.
[34] J. Liu, Y.-Q. Sun, H. Zhang, H. Shi, Y. Shi, W. Guo, *ACS Appl. Mater. Interfaces* **2016**, *8*, 22953–22962.
[35] M. Grzybowski, M. Taki, K. Kajiwara, S. Yamaguchi, *Chem. Eur. J.* **2020**, *26*, 7912–7917.
[36] J. Li, Y. Dong, R. Wei, G. Jiang, C. Yao, M. Lv, Y. Wu, S. H. Gardner, F. Zhang, M. Y. Lucero, J. Huang, H. Chen, G. Ge, J. Chan, J. Chen, H. Sun, X. Luo, X. Qian, Y. Yang, *J. Am. Chem. Soc.* **2022**, *144*, 14351–14362.
[37] A. Martin, P. Rivera-Fuentes, *bioRxiv Preprint* **2023**, https://doi.org/10.1101/2023.01.31.526423.
[38] A. Morozumi, M. Kamiya, S.-N. Uno, K. Umezawa, R. Kojima, T. Yoshihara, S. Tobita, Y. Urano, *J. Am. Chem. Soc.* **2020**, *142*, 9625–9633.
[39] X. Zhang, M. Zhang, Y. Yan, M. Wang, J. Li, Y. Yu, Y. Xiao, X. Luo, X. Qian, Y. Yang, *Chem. Commun.* **2021**, *57*, 7553–7556.
[40] X. Gu, E. Zhao, T. Zhao, M. Kang, C. Gui, J. W. Y. Lam, S. Du, M. M. T. Loy, B. Z. Tang, *Adv. Mater.* **2016**, *28*, 5064–5071.
[41] E. Komp, S. Valleau, *J. Phys. Chem. A* **2020**, *124*, 8607–8613.
[42] T. L. Greaves, K. S. Schaffarczyk McHale, R. F. Burkart-Radke, J. B. Harper, T. C. Le, *Phys. Chem. Chem. Phys.* **2021**, *23*, 2742–2752.

Manuscript received: April 30, 2023
Accepted manuscript online: May 28, 2023
Version of record online: ■■, ■■

Minireviews

Fluorescent Probes

W. Chi, D. Tan, Q. Qiao, Z. Xu,*
X. Liu* — **e202306061**

Spontaneously Blinking Rhodamine Dyes for Single-Molecule Localization Microscopy

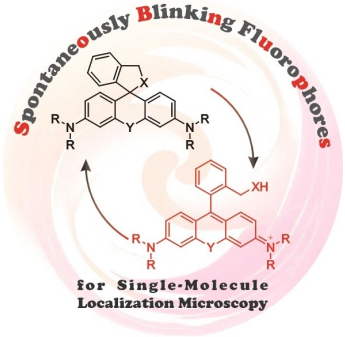

Spontaneously blinking fluorophores have the potential to significantly simplify experimental setups and extend the imaging duration of single-molecule localization microscopy. This review offers an overview of the development of spontaneously blinking rhodamines from 2014 to 2023, as well as an in-depth analysis of the mechanistic aspects of spontaneous blinking.